Al-rich AlGaN:Si layers and monolayer superlattices (digital alloys) (GaN/AlN):Si grown by plasma-activated molecular beam epitaxy

© A.N. Semenov, D.V. Nechaev, S.I. Troshkov, P.A. Alekseev, N.M. Shmidt, V.S. Kalinovskiy, V.N. Jmerik

Ioffe Institute,
St. Petersburg, Russia

E-mail: semenov@beam.ioffe.ru

Received Februrary 2, 2026
Revised May 15, 2026
Accepted May 15, 2026

The growth features of *n*-doped ultrashort-period monolayer superlattices GaN/AlN:Si superlattices — digital alloy with a minimum AlN (x) content of up to 85 %, which can replace conventional $Al_xGa_{1-x}N$:Si compounds with a similar x, using plasma-activated molecular beam epitaxy are described. It is shown that the original technology of pulsed plasma-activated molecular beam epitaxy in metal-rich conditions allows growing GaN_m/AlN_n digital alloys with layer thicknesses in monolayers (1 ML = 0.25 nm) $0.5 < m < 2$ ML, $2 < n < 6$ ML and a total thickness of ~ 500 nm. Digital alloys exhibit a planar, atomically smooth surface morphology with a root-mean-square roughness of < 0.39 nm over all scan areas up to $(10 \times 10)\,\mu m^2$. In contrast, AlGaN layers exhibit a grainy surface morphology with an average grain diameter of ~ 300 nm, resulting in an increase in root-mean-square surface roughness of > 2 nm over scan areas $\geq (3 \times 3)\,\mu m^2$. This difference is attributed to the different growth mechanisms of digital alloys and layers: while the former grows according to a two-dimensional nucleation mechanism, the latter follows a spiral growth mechanism. X-ray diffraction measurements revealed submonolayer (~ 0.3 monolayer) control accuracy for the thickness of GaN and AlN layers in digital solid solutions, ensuring x was specified with an accuracy of 3−7 %. Comparative studies of *n*-doping of GaN/AlN digital alloys with silicon demonstrated a maximum electron concentration of up to $\sim 10^{19}\,cm^{-3}$ for digital solid solutions with $x = 0.7$ and the possibility of obtaining conductive layers of digital solid solutions up to $x = 0.85$, while in $Al_xGa_{1-x}N$:Si layers with the same x, the electron concentrations were an order of magnitude lower and at $x > 0.8$, a semi-insulating nature of conductivity was observed. These results indicate the possibility of using *n*-doped digital alloys (GaN/AlN):Si with high x (up to 85 %) in device heterostructures.

Keywords: plasma-activated molecular beam epitaxy, digital alloys, wide bandgap semiconductors, monolayer superlattices, surface morphology, doping, AlGaN.

DOI: 10.61011/SC.2026.02.63749.9190

1. Introduction

For the last two decades globally the physics and technology of semiconductor optoelectronic devices of ultraviolet (UV) range are developing actively, and are supposed to substitute the currently widely used lamp mercury-containing devices. If semiconductor light-emitting and photodetection devices operating in the UV-A subrange of wavelengths $\lambda = 360-400$ nm, are already commercially manufactured, and their characteristics are close to record characteristics of similar devices of the visible subrange, for the devices of other UV-subranges (UV-B: $\lambda = 280-315$ nm and UV-C: $\lambda = 200-280$ nm) it cannot be stated [1]. Devices operating in these subranges are characterized with shorter service lives of devices and considerable (by orders of magnitude) fast degradation of characteristics that increases non-linearly as the wavelength shortens.

For development of the UV optoelectronics in the wavelength range from 200 to 355 nm, the most promising material base are wide-bandgap compounds of III group $Al_xGa_{1-x}N$, which form a continuous series of thermodynamically stable solid solutions in the entire range of compositions $x = 0-1$ with bandgap width from 3.4 to 6.1 eV accordingly. The first UVC light diodes were implemented in the beginning of 2000s [2], and currently the relevant objective for these instruments with working $\lambda \geq 265$ nm is to achieve in 2027 a quantum efficiency of ~ 30 %, which corresponds to the efficiency of lamp emitters ($\lambda = 253.7$ nm). Besides, today UVC photo- and light diodes operating in a so called „far UVC“ subrange of $\lambda < 240$ nm are in high demand. However, development of such UVC short wave instruments based on AlGaN-heterostructures with high content of AlN (> 70 %) compounds encountered serious problems in the production of highly conductive layers both with *p*- and *n*-type of conductivity, and also with the difficulties to make low ohmic contacts for them [3,4].

To solve the identified problems, one of the most promising approaches is replacement of solid solution AlGaN layers in instrument designs with ultra-short period superlattices $N \times (GaN_m/AlN_n)$, where N — number of periods, m and n — thicknesses of GaN and AlN layers expressed in monolayers (thicknesses of 1 ML ≈ 0.25 nm),

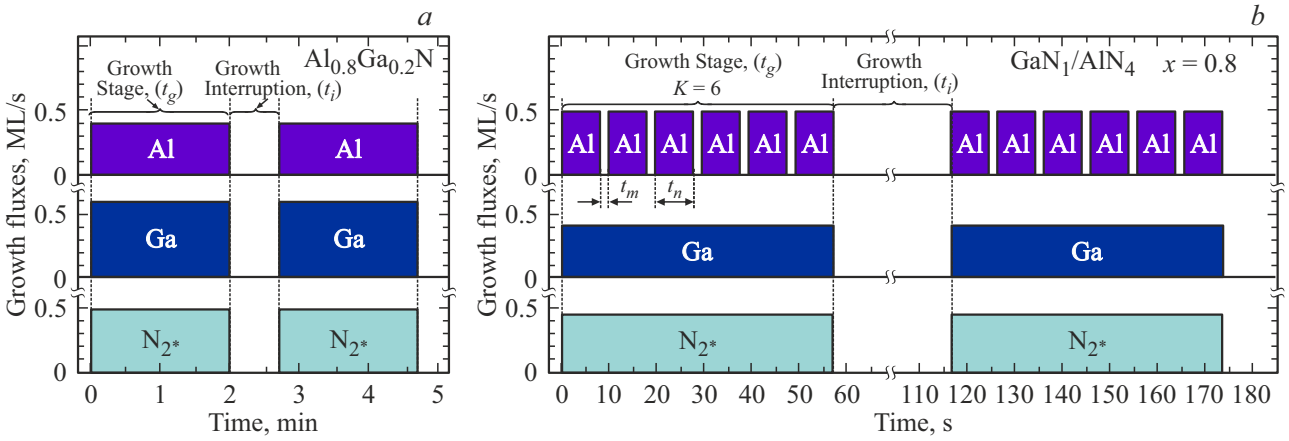

Figure 1. Timé diagrams of operation of growth source shutters in the PA MBE unit in growth of layer $Al_{0.8}Ga_{0.3}N$ by PMBE method (a) and DA $L \times \{6 \times (GaN_1/AlN_4)\}$ with the same $x = 0.8$ (b).

which are usually called digital alloys (DA) [5]. Typical values N are several hundreds, and values m and n vary from submonolayer level to several MLs. Such DAs have already been grown using ammonia molecular-beam epitaxy (MBE) in the beginning of 2000s by Temkin–Nikishin group to manufacture the first UVC light diodes and photo diodes [6,7]. Recently a group from the Nanjing University with the participation of H. Hirayma group [8] used plasma-activated MBE (PA MBE) to grow DAs GaN/AlN with record values of electron concentration $4.35 \cdot 10^{19}$ cm^{-3} and specific resistance of 0.036 Ohm $\cdot$ cm for DAs with average content of AlN 83 %.

This paper compares the mechanisms of epitaxial growth of volume layers in ternary alloys $Al_xGa_{1-x}N$:Si and DA $N \times (GaN_m/AlN_n)$:Si with high average content of AlN $x = 0.45-0.85$ on AlN/c-Al_2O_3 templates using pulse methods of plasma activated MBE (PA MBE) in metal-enriched environment. It is demonstrated that due to various growth mechanisms the DA layers have a substantially more planar atomically smooth topography of the surface compared to AlGaN layers of a close composition, the surface of which consists of individual grains with clear grain boundaries, which increases roughness RMS of the layers. Besides, most optimal parameters of DA with average content of AlN > 70 % are being discussed, which provide for their most effective donor doping with silicon.

2. Experiment

All samples of AlGaN layers and DAs were produced using PA MBE on a pre-annealed and nitridized substrates c-Al_2O_3 with AlN-bufer layers, the growth of which we described in paper [9]. First the nucleating layer of AlN was grown with thickness of 65 nm. For its growth the epitaxy was used with higher migration of atoms at substrate temperature $T_S = 780$ °C. Further growth of the buffer layer with thickness of up to $\sim 1.5\,\mu$m was carried out using metal-modulated epitaxy (MME) at variable ratio of Al and activated nitrogen flows $F_{Al}/F_{N_2} > 1.1$, which varied in accordance with the change of T_S from 780 to 850 °C. MME parameters prevented formation of metal (Al) drops and provides for the reduction of total concentration of growing dislocations to the level of $< 5 \cdot 10^9$ cm^2.

Thick layers of $Al_xGa_{1-x}N$:Si ($0.45 \le x \le 0.85$) with thickness of ~ 500 nm were grown at different values of $T_S = 680-710$ °C (with setting accuracy of ± 5 °C) in highly metal-enriched conditions with the ratio of total flow of III group atoms $F_{III} = F_{Al} + F_{Ga}$ and activated nitrogen $F_{III}/F_{N_2} \sim 2$. These conditions provided for the control of Al content using a simple ratio $x = F_{Al}/F_{N_2}$. To prevent formation of Ga drops, the technology of pulse MBE (PMBE) was used with short stops, the duration of which provided for complete desorption of excessive Ga with the desorption speed of $F^D_{Ga} = 0.15-0.42$ ML $\cdot$ s^{-1} in the corresponding temperature range of 680–710 °C [10]. Al desorption in this temperature range is practically absent. Timé diagrams of operation of each of the molecular beam shutters during PMBE of two periods in $Al_{0.8}Ga_{0.2}N$-layers are given in Figure 1, a.

Figure 1, b shows the operation of unit shutters in process of growth of two DA periods with $x = 0.8$ in the form of ultrashort-period superlattice $L \times \{K \times (GaN_m/AlN_n)\}$ at $m = 1$, $n = 4$, $K = 6$, where K — number of DA periods during each growth stage with the duration of t_g and interruptions between them lasting t_i, L — number of growth stages in the DA layer. For variation of x within 0.7 to 0.85 the DA parameters changed within $0.5 \le m \le 2$ ML, $2 \le n \le 6$ ML, and the average composition was controlled using formula $x = n/(m+n)$. All DA layers had approximately the same thickness of 500 nm, which was achieved through corresponding change of the total number of periods using formula $N = K \cdot L$, $K = 6.20$, $L = 32-48$. DA growth was happening only during the growth stage noted in the figure with continuously open shutters of nitrogen and gallium flows. The position of the Al-source shutter varied periodically, and in the open position the

AlN-layers were growing with simultaneous accumulation of excessive Ga, and when it closed, GaN layers were grown. The growth of GaN/AlN with the simultaneous presence of Ga and Al adatoms on the surface is based on incorporation in exclusively Al atoms into the lattice with complete suppression of Ga atoms incorporation in as a result of higher bond energy in AlN (2.88 eV) compared to GaN (2.24 eV) [11]. To prevent growth of AlGaN layer instead of the specifeid AlN layer and precise control of GaN-insert thicknesses, it is necessary to precisely maintain the ratio $F_{\mathrm{Al}}/F_{\mathrm{N_2}} \geq 1$. Since the growth of both layers in DA was happening in metal-enriched conditions, their thicknesses were defined by simple ratio $m(n) = F_{\mathrm{N_2}} \times t_{m(n)}$, where $t_{m(n)}$ — duration of closing (opening) of the Al-source shutter, $F_{\mathrm{N_2}} = 0.45{-}0.5$ ML/s with accuracy of maintaining in $0.02\,\mathrm{ML}\cdot\mathrm{s}^{-1}$ within a single process. During the stop of DA growth for the time t_i, complete desorption of excessive Ga accumulated during the growth stage was taking place. All layers and DAs were continuously doped with silicon using a standard solid state source.

The growth of the samples was continuously controlled *in situ* using reflection high-energy diffraction (RHED) and laser reflectometry. The morphology of the grown layers and DAs were studied using a scaning electron and an atomic force microscropes (SEM and AFM, accordingly). The average composition of the layers and thicknesses of layers in DA were assessed using X-ray diffraction measurements conducted on a unit of JSC Research Center „Burevestnik" DRON 8T. Concentrations of charge (electron) carriers in the layers were defined using $C{-}V$-method with a mercury probe. Besides, the spreading resistance (R_{sp}) was measured between two drops of In with the values of diameters and distances between them of 2 and 5 mm, accordingly.

3. Results and discussion

3.1. Mechanisms for growth of AlGaN layers and digital alloys GaN/AlN

Difficulties of epitaxial growth of the layers of Al-containing nitride compounds of group III are caused by several problems. First of all, they are related to low surface mobility of Al adatoms, which results in the need to increase the growth temperatures of Al-containing compounds. However, in highly vacuum conditions of PA MBE ($< 5 \cdot 10^{-5}$ Torr) the capabilities of increasing the growth temperatures are limited to limit values of growth flows restricted to the violation of the molecular mode of their flow in a growth chamber. Therefore, in this paper to solve this problem, the alternative methods of layer and DA growth in metal(Ga)-enriched conditions were used, under which a bilayer Ga-adlayer is formed on the surface of growing layers, which provides for higher mobility of adatoms [12]. Besides, the production of structurally perfect layers of ternary compound AlGaN is complicated with a significant difference in the energy barriers of the surface diffusion of Al (1.17 eV) and Ga (0.99 eV) adatoms [13], whcih causes disturbances in the layerwise growth with the homogeneous spatial distribution of cation atoms. And finally let us note the spontaneous formation of superlattice structures in AlGaN-layers, which is explained by the features of growth of these compounds with the hexagonal structure of the lattice [14].

Figure 2 shows SEM- and AFM-images of the surface of $\mathrm{Al_{0.7}Ga_{0.3}N}$ layer grown with the help of PA MBE, which is characterized by formation of grains with typical diameter of ~ 300 nm and deep grain boundaries with depth of down to 10 nm. As a result, these layers demonstrate relatively high root mean square (RMS) roughnesses of the surface, reaching the same value of ~ 2.1 nm at scanning areas of 3×3 and $10 \times 10\,\mu\mathrm{m}^2$. In process of AFM-scanning within the grain in the surface area of $500 \times 500\,\mathrm{nm}^2$ the RMS roughness values were 1.8 nm. Figures 2, *c* and *d* show that the grains have a stepwise topography with flat terraces having width of $\sim 30{-}40$ nm and step height of ~ 2 ML. The atomically smooth topography of terraces was confirmed by linear RHED pattern observed continuously during layer growth and shown in the insert to Figure 2, *a*.

The results of these studies confirm the growth of AlGaN-layers in accordance with the classic helical (stepwise-layer) growth mechanism of Burton–Cabrera–Frank [15], which is usually implemented in the metal-enriched conditions of layer growth III-N with the ratio of $(F_{\mathrm{III}}{-}F_{\mathrm{III}}^{\mathrm{D}})/F_{\mathrm{N}} > 1$ flows and with high concentration of growing dislocations with the screw component [16].

The results of our prior research [9] of the growth using MME for the binary GaN and AlN layers also show the helical growth mechanism, but the typical diameter of the grains in them compared to AlGaN is larger and reaches $\sim 1\,\mu$m. It seems that this difference in the morphology of the surface results in the substantially higher values of surface roughness (RMS > 1.8 nm) in AlGaN layers compared to similar characteristics of the binary layers, for which the typical values are RMS < 1 nm [9].

The difference between the morphologies of AlN and AlGaN layers, in our opinion, is first of all related to the difference of temperatures of their growth that was $\sim 150\,^{\circ}$C. Since this temperature through Arrhenius equation defines the equilibrium pressure for the growing layer (P_{eq}), you can expect substantially lower values (by several orders of magnitude) for low temperature AlGaN layers. The value of the critical (maximum achievable) radius of grains (ρ_c) in process of helical growth is inversely proportional to the logarithm of oversaturation of growth flows $\rho_c \sim 1/\ln(\xi + 1)$, where $\xi = (P/P_{\mathrm{eq}}) - 1$ — oversaturation of the growth flow [17]. Accordingly, reduction of P_{eq} for AlGaN-layers must result in the reduction of ρ_c, and this is observed experimentally (Figure 2, *b* and Figure 6, *d* in paper [9]). For the GaN and AlGaN layers grown at the same temperature ($\sim 700\,^{\circ}$C) the large diameter of grains is first explained by hígh equilibrium pressure of this binary compound compared to equilibrium pressure of the ternary compound [10]. Variation of the growth temperature of $\mathrm{Al}_x\mathrm{Ga}_{1-x}\mathrm{N}$ ($x > 0.7$) layers within 660 to 720 °C with

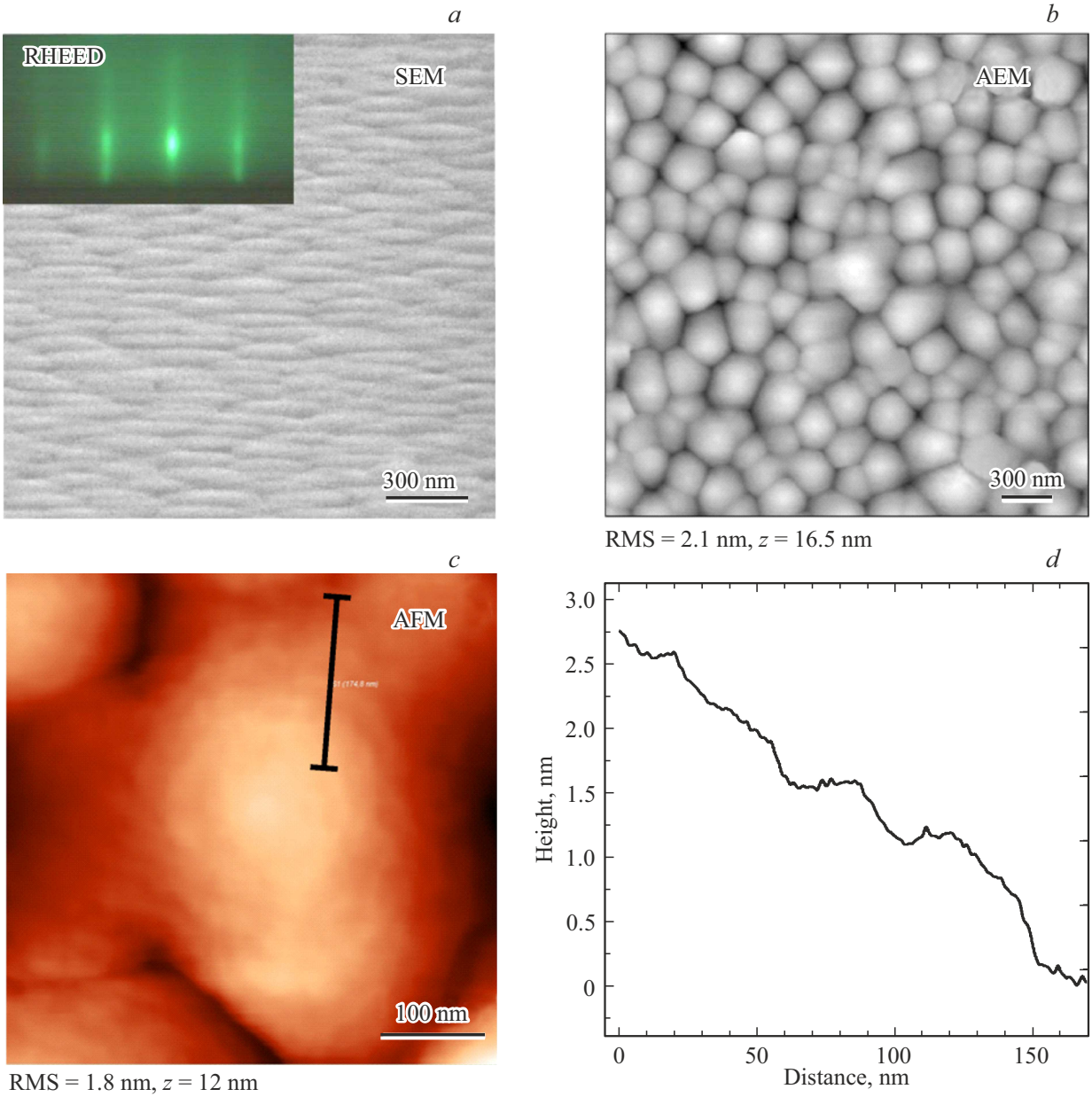

Figure 2. AFM- and SEM-images of the $Al_{0.7}Ga_{0.3}N$:Si solid solution layer surface with thickness of 500 nm, grown on the AlN/c-Al_2O_3 template using PMBE.

preservation of metal-enriched conditions did not vary the nature of layer topography, but resulted only in a small increase of the grain radius and width of grain boundaries.

Contrary to AlGaN layers with the granular morphology of the surface all GaN/AlN DAs demonstrated in SEM- and AFM-images the planar and grain-free morphology of the surface as shown in Figure 3.

Among potential microdefects observed in DAs, let us note the presence of traces of a microdrop metal phase shown in Figure 3, a on the surface of some samples. These microdefects were formed in process of growth under metal-enriched conditions in case of failure to comply with the balance between the quantity of Ga accumulated on the surface during the growth stage $Q_{\mathrm{Ga}}^{\mathrm{exc}} = (F_{\mathrm{Ga}} - F_{\mathrm{Ga}}^{\mathrm{D}}) \cdot t_g - K \cdot F_{\mathrm{N}_{2*}} \cdot t_m$ and the quantity of Ga desorbed during growth interruption $Q_{\mathrm{Ga}}^{\mathrm{D}} = F_{\mathrm{Ga}}^{\mathrm{D}} \cdot t_i$. The surface morphology shown in Figure 3, a was observed for the DA $32 \times \{20 \times (\mathrm{GaN}_{0.98}/\mathrm{AlN}_{2.25})\}$:Si, and the calculations using these formulae show that this growth complied with inequation $Q_{\mathrm{Ga}}^{\mathrm{exc}} > Q_{\mathrm{Ga}}^{\mathrm{D}}$. However, for DA $45 \times \{20 \times (\mathrm{GaN}_{0.50}/\mathrm{AlN}_{2.0})\}$, which shows planar atomically smooth morphology shown in Figure 3, c, d, the calculations show compliance with inequation $Q_{\mathrm{Ga}}^{\mathrm{exc}} < Q_{\mathrm{Ga}}^{\mathrm{D}}$, which indicates complete desorption of excessive Ga, when growth stops. Note also low RMS roughnesses of the DA surface, amounting to 0.32 and 0.39 nm for scanning areas of

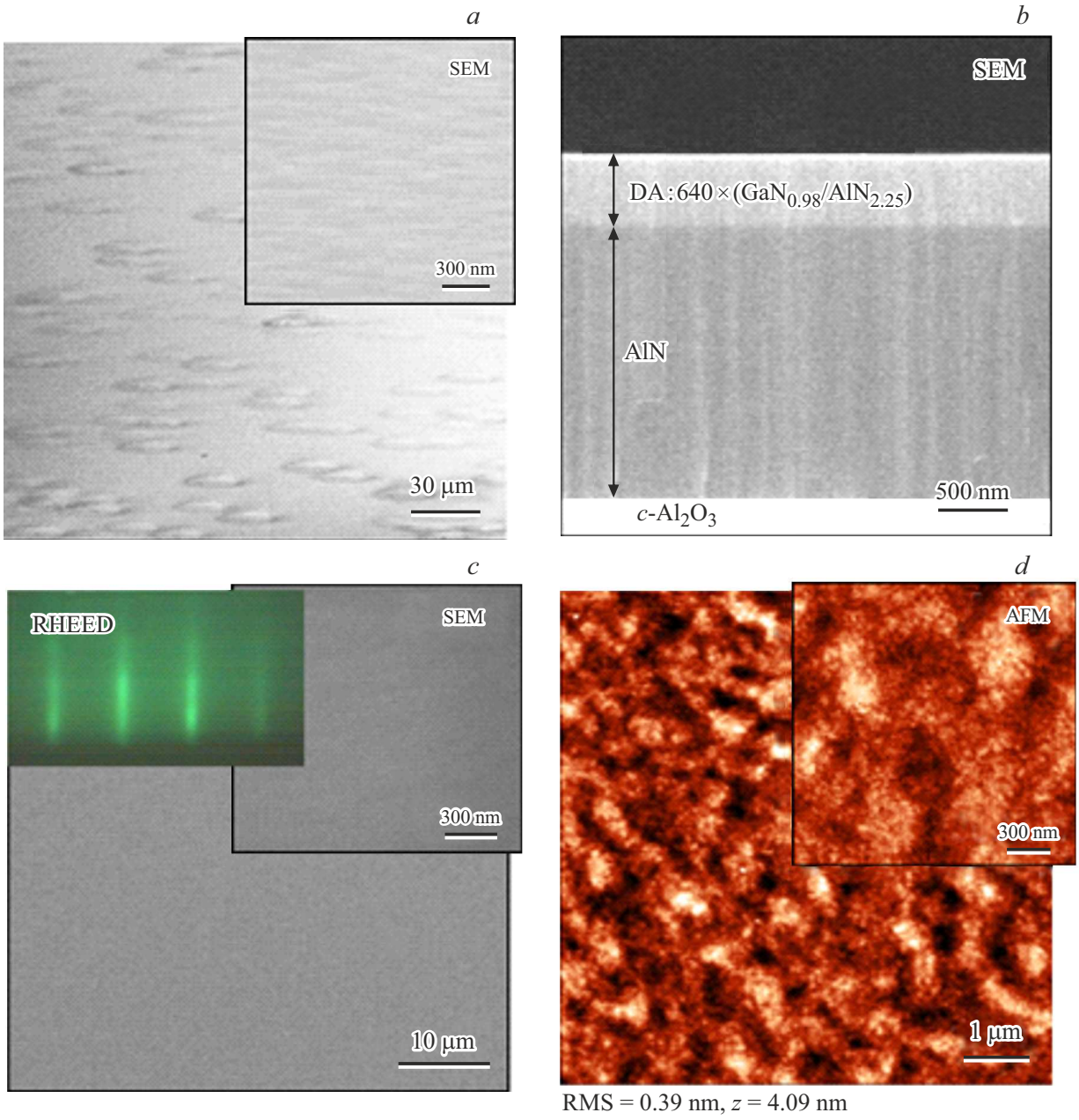

Figure 3. The AFM- and SEM-images of the DA layer surface with thickness of $\sim$ 500 nm and $x = 0.7$, grown under different conditions: $32 \times \{20 \times (GaN_{0.98}/AlN_{2.25})\}$ at $Q_{Ga}^{exc} > Q_{Ga}^{D}$ (a, b) and $45 \times \{20 \times (GaN_{0.50}/AlN_{2.0})\}$ at $Q_{Ga}^{exc} < Q_{Ga}^{D}$ (c, d).

3×3 and $10 \times 10\,\mu m^2$, accordingly, which is substantially lower than the simiilar characteristics of $Al_{0.7}Ga_{0.3}N$ layers.

The substantial difference in morphologies of AlGaN layers and GaN/AlN DAs with approximately same thicknesses ($\sim$ 500 nm) and average content of AlN ($x \sim 0.7$) indicates a fundamental difference in the growth mechanisms of these layers, despite the use of approximately the same metal(Ga)-enriched conditions during their growth with values of $F_{III}/F_{N_2} \sim 2$ and $T_s \sim 690-700\,^{\circ}C$. If in the first case the layers show all main signs of helical growth, the surface of DA layers demonstrates complete absence of any signs of this growth mechanism, and the topography of these objects corresponds to 2D-nucleation growth mechanism.

Potential transition from the stepwise-laminar helical mechanism of epitaxial layer growth to 2D-nucleation growth mechanism was theoretically described in paper [18]. In this paper this transition was related to introduction of elastic stresses in growing heterostructures, which change the thermodynamics/kinetics of formation of steps and nucleation processes of 2D-islands on the terraces in process of stepwise-laminar growth. Therefore, you can assume the relation of the observed differences in the growth mechanisms in AlGaN layers and GaN/AlN DAs to the

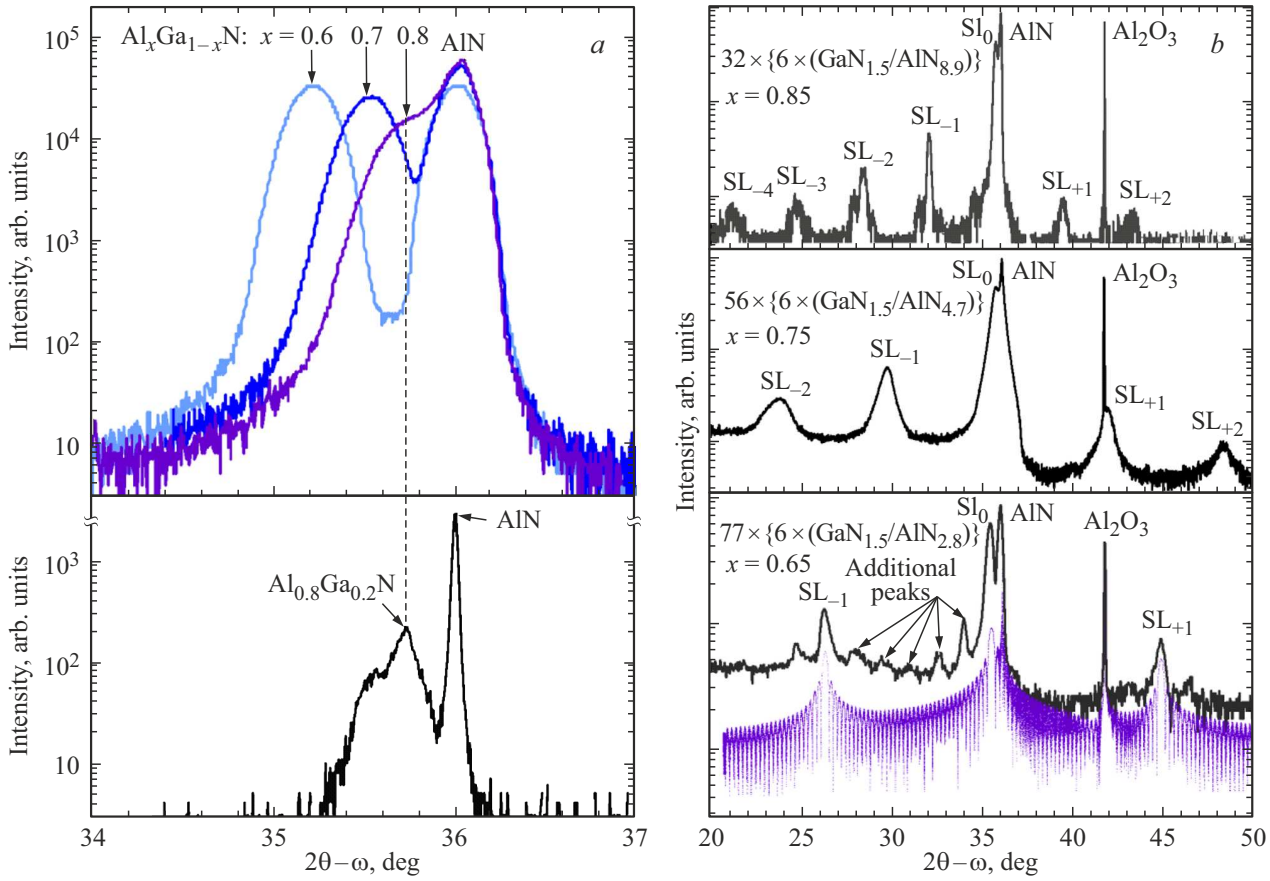

Figure 4. X-ray diffraction curves obtained in the mode of 2θ-ω scanning for $Al_xGa_{1-x}N$ (a) layers and $K \times \{L \times (GaN_m/AlN_n)\}$ (b) DAs with different composition in the range of $x = 0.6-0.85$.

different nature of generation and evolution of elastic stresses in these objects.

Besides, it is necessary to account for the potential difference between the thermodynamic and kinetic features of formation of these objects. When AlGaN-layers grow, Al, Ga atoms are simultaneously incorporate into the lattice of the AlGaN-layer, which results in the formation of spatial irregularities of the composition, causing reduction in the surface mobility of adatoms. Nevertheless, due to Ga-enriched conditions, the growth of the ternary compound layers happens in accordance with the helical mechanism. In process of DA growth, alternating growth of binary multi-layer AlN and GaN takes place under the conditions of strong oversaturation with group III atoms (Ga) and continuous generation of sign-alternating stresses due to crystallographic mismatch between these layers. All of this is likely to provide for the 2D-nucleation mechanism of DA growth, but for more accurate and thorough description of this phenomemon, further experimental and theoretical studies are necessary.

3.2. X-ray diffraction studies

The compliance between the specified and measured values of AlGaN layers and GaN/AlN DAs parameters (the difference of these values is further called precision) in the area of average compositions $x = 0.6-0.8$ was tested using X-ray diffraction measurements of 2θ-ω curves. Figure 4, a shows 2θ-ω curves of $Al_xGa_{1-x}N$ layers measured using a two-crystal geometry, which shows that as the aluminum content increases, the diffraction peaks from the $Al_xGa_{1-x}N$ layers approach the AlN peak, but after reaching $x = 0.8$ further determination of the composition is difficult. Therefore, in this area of compositions it is necessary to use three-crystal geometry of measurements with hígh angular resolution, which is provided in the lower panel of Figure 4, a. The average compositions of the layers determined in this manner in the assumption of their coherent growth are given in the table. These values demonstrate good ($\leq 1\,\%$) agreement with the specified values $x = F_{Al}/F_{N_2}$.

Figure 4, b shows 2θ-ω curves for several GaN_m/AlN_n DAs with somewhat worse precision of determination of superlattice parameters, which are given in the table. The results of modeling of one of rocking curves used to determine parameters of DA lattice, are given in the lower panel of Figure 4, b. For DAs the precision of determination of their average compositions was $3-7\,\%$, which was provided for by average precision of ~ 0.3 ML

Nominal and experimentally measured values of parameters of AlGaN layers and GaN/AlN DAs

	Thickness of GaN, ML		Thickness of AlN, ML		DA period, ML		Al content (x)	
	Nominal	Experiment	Nominal	Experiment	Nominal	Experiment	Nominal	Experiment
$Al_{0.6}Ga_{0.4}N$	–	–	–	–	–	–	0.60	0.61
$Al_{0.7}Ga_{0.3}N$	–	–	–	–	–	–	0.70	0.70
$Al_{0.8}Ga_{0.2}N$	–	–	–	–	–	–	0.80	0.81
DA-65 %	1.5	1.2	2.8	2.7	4.3	3.9	0.65	0.68
DA-75 %	1.5	1.1	4.7	2.7	6.2	6.1	0.75	0.82
DA-85 %	1.5	1.3	8.9	9.2	10.3	10.5	0.85	0.88

(~ 0.0762 nm) in the determination of the thickness of GaN and AlN layers in the DAs. These errors, in our opinion, arise for several reasons, including potential discrepancies in the calibration of growth flows used to specify the lattice parameters, and also consistent errors of X-ray diffraction measurements of ultrathin layers of DAs with submonolayer precision, which we described in paper [19].

It is important to note that the experimental 2θ-ω curve for $77 \times \{6\times(GaN_{1.2}/AlN_{2.7})\}$ ($x = 0.68$) DA shown in the lower panel of Figure 4, *b* shows additional peaks that correspond to the formation of the periodical structure with a noticeably hígher period equal to the thickness of six periods specified by DA. Appearance of these features may be explained by parasitic growth of superthin GaN inserts in process of periodical stops of growth after the growth of each 6 periods of DA. This growth is caused by parasitic flow of plasma-activated nitrogen from under the nominally closed shutter of the plasma source. The absence of the signs of additional periodical structure formation in two other structures seems to be related to a smaller number of the periods in them. In any case these results indicate the need for further optimization of the DA growth processes in the Ga-enriched conditions.

3.3. Measurements of electrophysical characteristics

Measured electrophysical characteristics of $Al_xGa_{1-x}N$:Si layers confirmed the well-known complexity of donor doping in the layers with high x. Figure 5, *a* shows drastic reduction of electron concentration in the layers at $x > 0.55$ until the semi-insulating behavior at $x > 0.8$, which agrees with the data of the review articles [3,4]. Note good agreement between the measured $C-V$-method electron concentrations and values of spreading resistance (R_s), which were determined from the measurement of current-voltage curves of conductivity between In-contacts on the surface. Dependences shown in Figure 5, *c* R_s on the temperature of the silicon effusion source (silicon flow) demonstrate the possibility of conductivity control of $Al_xGa_{1-x}N$:Si layers until the maximum value of $x = 0.7$. Measurements of spreading resistance for $Al_{0.8}Ga_{0.2}N$:Si-layer were single, therefore at smaller Si flows there was no conductivity of the layers.

According to the literature data, these results correspond to both the icnrease of impurity ionization energy observed at $x > 0.8$ and are also due to non-linear increase of concentrations of various defects that decrease the electron concentration. The speed of generation of these defects increases sharply already upon achievement of the critical concentration $x \sim 0.6$. These defects in AlGaN:Si layers include deep DX-centers compensating defects in the form of cation vacancy complexes V_{III}-Si and impurity carbon atoms.

Optimization of AlGaN layer growth conditions with high Al to minimize the concentrations of the defects is a complicated task, since these defects demonstrate complex and often opposite dependences of energy of their formation on the growth parameters. Besides, it is necessary to account for the limitations in the selection of growth modes of PA MBE, among which let us note, for example, the inability to use nitrogen-enriched conditions of growth during the growth of the layers in the active and subcontact areas of instrumental heterostructures, since this results in the disturbance of the planarity of the surface morphology of these layers. On the other hand, the use of too strong metal-enriched conditions may result in the substantial increase of leakage currents in the instrumental heterostructures.

Figure 5, *b* shows the dependence of electron concentration in the DA series with the same $x = 0.7$, but different values of thicknesses of $m = 0.7-2$ ML and $n = 1.5-4.7$ ML layers. It leads to the conclusion on the more effective doping of DA with bilayer and fractional thicknesses of GaN:Si-layers compared to the DA with mono- and submonolayer thicknesses of these layers. The maximum value of electron concentration $1 \cdot 10^{19}$ cm^{-3} is observed in $21 \times \{20 \times (GaN_2/AlN_{4.5})\}$:Si with $x = 0.7$, whereas in the layer $Al_{0.7}Ga_{0.3}N$:Si the concentration of electrons is by an order less ($\sim 1.2 \cdot 10^{18}$ cm^{-3}).

Relatively low values of R_s in Figure 5, *d* measured for various DAs with the maximum value of $x = 0.85$ in $GaN_{1.5}/AlN_{8.9}$ (according to the table with the data of X-ray diffraction measurements, the value of x in this DA was 0.88), indicate a relatively effective transport of carriers through tunnel-transparent dielectric AlN layers with thicknesses of up to ~ 9 ML, which causes relatively high DA conductivity. Note that as the Si flow grew in the range that we studied, being limited by maximum

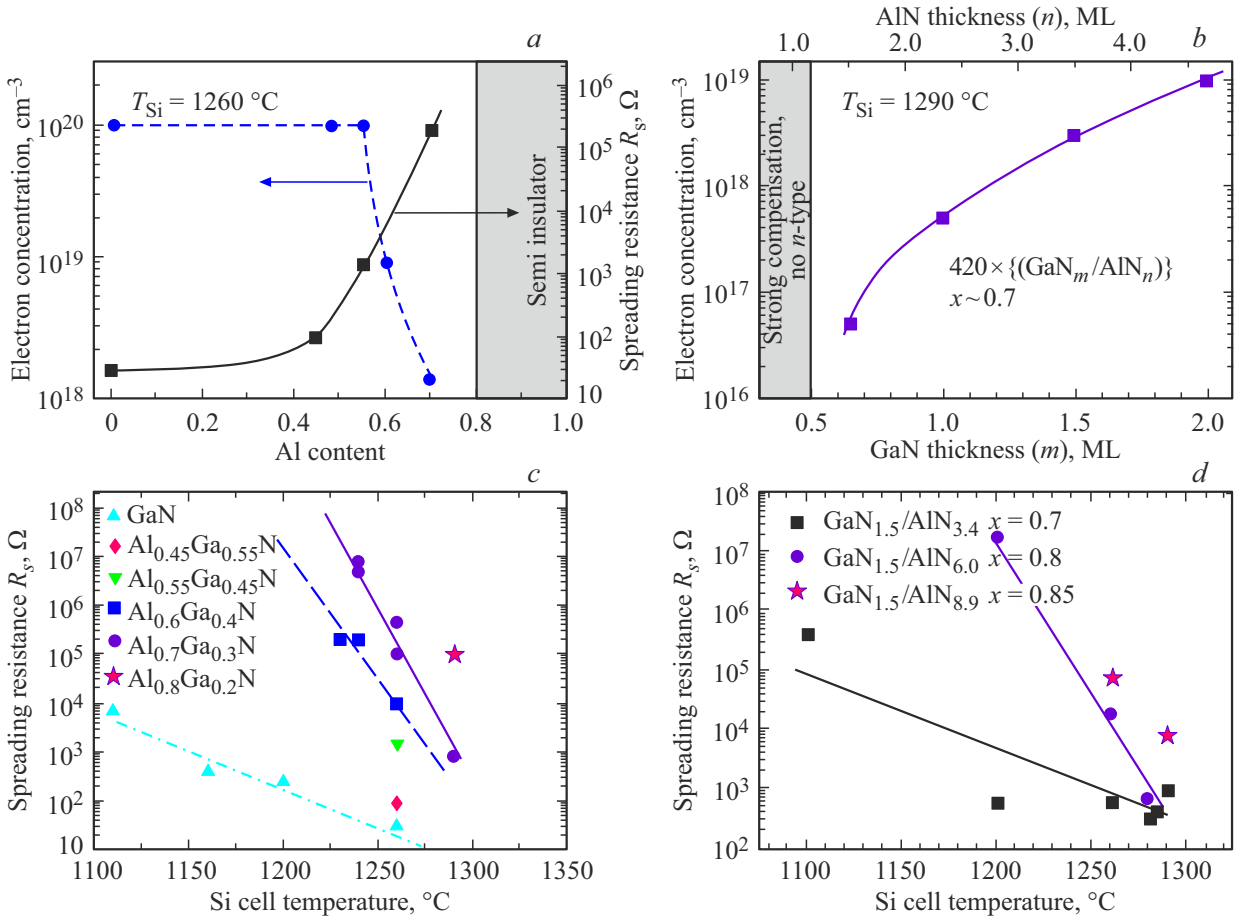

Figure 5. *a* — dependences of electron concentration and spreading resistance in $Al_xGa_{1-x}N$:Si layers on the content of aluminum ($x = 0-0.7$). *b* — dependence of concentration of electrons in DA GaN_m/AlN_n:Si with constant $x = 0.7$ and thickness of ~ 500 nm on thickness of GaN and DA (m). Dependences of spreading resistances for $Al_xGa_{1-x}N$:Si (*c*) layers and GaN_m/AlN_n:Si (*d*) DA with different $x = 0.45-0.85$ on the temperature of the effusion source of silicon (Si flow).

temperature of the used effusion cell, only the improvement of the doping characteristics was observed, which makes it possible to assume minor concentrations of DX-defects in the DA.

4. Conclusion

The paper demonstrated the promising outlook of using n-doped DAs on the basis of ultrashort-period superlattices $N \times (GaN_m/AlN_n)$:Si with the total thickness of several hundreds nm and controlled average content of AlN 40–85% as the alternative to standard layers of the ternary solid solution $Al_xGa_{1-x}N$:Si with the similar composition. The fundamental difference was found in the mechanisms of epitaxial growth of AlGaN layers and GaN/AlN DA with the use of pulse methods of PA MBE under the metal-enriched conditions. It is shown that the growth of all DAs happens in accordance with the 2D-nucleation mechanism, whereas the growth of AlGaN layers happens in accordance with the stepwise-laminar (helical) mechanism. This difference results in the substantial difference of surface charactteristics of DAs and layers. If the first show planar atomically smooth morphology of the surfaces with roughness RMS of < 0.4 nm in all surface areas of AFM scanning of $< 10 \times 10\,\mu m^2$, the AlGaN layers of the same composition demonstrate typical RMS of > 2 nm. Donor doping of $Al_xGa_{1-x}N$:Si layers found drastic reduction of electrons in the layers with $x > 0.55$ from $\sim 10^{20}$ to $\sim 1 \cdot 10^{18}$ cm^{-3} at $x = 0.7$, whereas DAs with the similar AlN content had electron concentration of up to $\sim 1 \cdot 10^{19}$ cm^{-3}. Besides, semi-insulating nature of conductivity of $Al_xGa_{1-x}N$ layers with $x > 0.8$ was demonstrated, as well as n-conductivity in the DA with the maximum value of $x = 0.85$.

Funding

A.N. Semenov and D.V. Nechaev would like to thank the Russian Scientific Foundation for the support of the studies, grant No. 25-22-00898 (https://rscf.ru/project/25-22-00898/).

Conflict of interest

Authors declare no conflict of interest.

References

[1] H. Amano, R. Collazo, C.D. Santi, S. Einfeldt, M. Funato. J. Phys. D: Appl. Phys., **53**, 503001 (2020). DOI: 10.1088/1361-6463/aba64c

[2] V. Adivarahan, J. Zhang, A. Chitnis, W. Shuai, J. Sun, R. Pachipulusu, M. Shatalov, M.A. Khan. Jpn. J. Appl. Phys., **41**, L 435 (2002). DOI 10.1143/JJAP.41.L 435

[3] Y.-H. Liang, E. Towe. Appl. Phys. Rev., **5**, 011107 (2018). DOI: 10.1063/1.5009349

[4] J. Wang, F. Xu, L. Zhang, J. Lang, X. Fang, Z. Zhang, X. Guo, C. Ji, C. Ji, F. Tan, X. Yang, X. Kang, Z. Qin, N. Tang, X. Wang, W. Ge, B. Shen. J. Semiconductors, **45**, 021501 (2024). DOI: 10.1088/1674-4926/45/2/021501

[5] M. Asif Khan, J.N. Kuznia, D.T. Olson, T. George, W.T. Pike. Appl. Phys. Lett., **63**, 3470 (1993). DOI: 10.1063/1.110123

[6] G. Kipshidze, V. Kuryatkov, B. Borisov, M. Holtz, S. Nikishin, H. Temkin. Appl. Phys. Lett., **80**, 3682 (2002). DOI: 10.1063/1.1480886

[7] S.A. Nikishin. Appl. Sci., **8**, 2362 (2018). DOI: 10.3390/app8122362

[8] S. Li, X. Liang, P. Shao, S. Chen, Z. Li, X. Su, T. Tao, Z. Xie, M.A. Khan, L. Wang, T.T. Lin, H. Hirayama, B. Liu, D. Chen, K. Wang, R. Zhang. Appl. Phys. Lett., **125**, 112102 (2024). DOI: 10.1063/5.0215886

[9] D.V. Nechaev, O.A. Koshelev, V.V. Ratnikov, P.N. Brunkov, A.V. Myasoedov, A.A. Sitnikova, S.V. Ivanov, V.N. Jmerik. Superlat. Microstr., **138**, 106368 (2020). DOI: 10.1063/5.0215886

[10] V.N. Jmerik, D.V. Nechaev, S.V. Ivanov. *Molecular Beam Epitaxy: from Research to Mass Production*. 2nd edn, ed. by M. Henini (Amsterdam–Netherlands–Oxford, UK, Cambridge, USA, Elsevier Inc., 2018) p. 135. ISBN: 9780128121368. DOI: 10.1016/B978-0-12-812136-8.00008-6

[11] W.A. Harrison. *Electronic Structure and the Properties of Solids* (Dover, N.Y., 1989) p. 176.

[12] J.E. Northrup, J. Neugebauer, R.M. Feenstra, A.R. Smith. Phys. Rev. B, **61**, 9932 (2000). DOI: 10.1103/PhysRevB.61.9932

[13] V. Jindal, F. Shahedipour-Sandvik. J. Appl. Phys., **105**, 084902 (2009). DOI: 10.1063/1.3106164

[14] M. Gao, S.T. Bradley, Y. Cao, D. Jena, Y. Lin, S.A. Ringel, J. Hwang, W.J. Schaff, L.J. Brillson. J. Appl. Phys., **100**, 103512 (2006). DOI: 10.1063/1.2382622

[15] W.K. Burton, N. Cabrera, F.C. Frank. Phil. Trans. R. Soc. London, Ser. A, **243**, 299 (1951). DOI: 10.1098/rsta.1951.0006

[16] B. Heying, E.J. Tarsa, C.R. Elsass, P. Fini, S.P. DenBaars, J.S. Speck. J. Appl. Phys., **85**, 6470 (1999). DOI: 10.1063/1.370150

[17] Y. Cui, L. Li. Phys. Rev. B, **66**, 155330 (2002). DOI: 10.1103/PhysRevB.66.155330

[18] C. Ratsch, M.D. Nelson, A. Zangwill. Phys. Rev. B, **50**, 14489 (1994). DOI: 10.1103/PhysRevB.50.14489

[19] V. Jmerik, D. Nechaev, K. Orekhova, N. Prasolov, V. Kozlovsky, D. Sviridov, M. Zverev, N. Gamov, L. Grieger, Y. Wang, T. Wang, X. Wang, S. Ivanov. Nanomaterials, **11**, 2553 (2021). DOI: 10.3390/nano11102553

Translated by M.Verenikina